

TA  
710.2  
.S25  
2010

**OPTICAL MEASUREMENT OF SAND DEFORMATION AROUND AN UPLIFTING  
DEEP ANCHOR USING DIGITAL IMAGE CORRELATION METHOD**

By

Pezhman Sainia (B.Sc)

at Ryerson University, April 2010

A Project presented to Ryerson University in partial fulfillment of the requirements for the degree of Master of Engineering In the program of Civil Engineering

Toronto, Ontario, Canada, 2010

©(Pezhman Sainia) 2010

PROPERTY OF  
RYERSON UNIVERSITY LIBRARY

I hereby declare that I am the sole author of this project.

I authorize Ryerson University to lend this project to other institutions or individuals for the purpose of scholarly research.

I further authorize Ryerson University to reproduce this project by photocopying or by other means, in total or in part, at the request of other institutions or individuals for the purpose of scholarly research.

# TABLE OF CONTENTS

TABLE OF CONTENTS.....	iii
ACKNOWLEDGEMENTS.....	iv
NOTATIONS.....	v
ABSTRACT.....	vi
1. INTRODUCTION.....	1
1.1    General	1
1.2    Applications	4
1.3    Scope and Study Method	6
2. SOIL PROPERTY AND EXPERIMENT SETUP.....	7
2.1    Experimental Set-up	9
2.2    Soil Property	11
3. SCALED MODEL TEST PREPARATION.....	12
4. DIGITAL IMAGE CORRELATION PROCESSING TECHNIQUE.....	15
4.1    General Theory	15
4.2    Theory of DIC	16
4.3    Data Processing	18
5. RESULT ANALYSIS.....	20
5.1    Theatrical Solution to the anchor problem	20
5.2    Model Test Result of an Anchor in Dense Sand	21
5.2.1    Force vs. Displacement in Dense Sand	21
5.2.2    Displacement Field in Dense Sand Using DIC Method	23
5.2.3    Shear Strain in Dense Sand	24
5.3    Model Test Results of an Anchor in Loose Sand	26
5.3.1    Force vs. Displacement in Loose Sand	26

5.3.2	Displacement Field in Loose Sand Using DIC Method	27
5.3.3	Shear Strain in Loose Sand	29
5.4	A Comparison between Pullout Resistances in This Research Study and the Work of Others	32
6.	CONCLUSION.....	33
	REFERENCES.....	34

## ACKNOWLEDGEMENTS

I wish to express my deepest appreciation to my advisor, Dr. Jinyuan Liu, at Ryerson University, for his constant support and valuable inputs during the development of this research. Dr. Liu devoted his time and effort to make this study a success. His most helpful guidance is greatly appreciated.

## NOTATIONS

$C_u$	Uniformity Coefficient
$C_c$	Coefficient of curvature
$d$	Displacement
$D_R$	Relative Density
$D$	Anchor Diameter
$F$	Pull out force
$F_y$	Basic Capacity Factor
$F'_y$	Anchor Capacity Factor
FL	Fine Loose Sand
FD	Fine Dense Sand
H	Height of embedment
$K_o$	Correction Factors for the Effect of Soil
t	Time
$q_u$	Average Applied Pressure
$R_\psi R_R R_k$	Correction Factors
$\gamma_{dmax}$	Max dry unit weight
$\gamma_{dmin}$	Min dry unit weight
$\gamma_d$	Sample dry unit weight
$\phi$	Angle of Friction
$\delta_f$	Anchor displacement

## **Abstract:**

This report presents a study on the soil deformation around an uplifting deep circular anchor in sand. A scaled model anchor test setup, including a loading frame, a Plexiglas mould, a camera, and a computer, was developed and a series of scaled model test were performed in order to investigate the mechanical behavior and failure modes of a deep anchor embedded in sand. To find the displacement field the digital image correlation (DIC) method was applied. A set of images were captured while a semi-circular anchor was uplifted against the Plexiglas window, and soil displacement field was calculated by comparing any two consecutive images using DIC method. The study shows that the density of soil has a significant effect on both the deformation characteristics and the failure mechanism of the anchor. While in loose sand the failure zone is a compressed bell shape, in dense sand the failure zone is a truncated cone extending from the anchor edge to the surface of the soil. Furthermore, in dense sand the anchor experiences smaller displacement before reaching to the peak pullout force compared to a larger displacement in loose sand. This report has been done by Pezhman Sainia for the M.Eng degree's research project final report with the supervision of Dr. Jinyuan Liu.

# CHAPTER 1

## INTRODUCTION

### 1.1 General

Different types of anchorage systems are used to stabilize structures, such as power transmission structures, tunnels and offshore structures, against uplifting loads. Using anchorage systems also increases the compression capacity of the ground. Anchors also have numerous applications in structures such as television and transmission towers, tension cables for suspension bridges, and tent type roofs. These types of structures may experience large uplift forces on their foundations when subjected to the wind load.

With the extensive use of anchors, the understanding of their behavior has attracted the attentions of researchers for more than half a century. The performance of an anchor is affected by many factors including the geometry of anchor, soil conditions/properties, depth of anchor burial, etc. Anchoring properly secures structures against vertical displacement under uplift and overturning forces, and also against tangential displacement or shear failure along a critical/weak surface in the subsoil. (Leos Hobst and Josef Zajic 1977)

Sutherland (1965) found that the mode of rupture varies with density of sand. McDonald (1963) found out that for shallow depths of embedment, the failure surface shape was almost parabolic. Dickin and Leung (1990) proved that anchor geometry has a significant influence on the failure modes. They used layers of sand with different colors in their experiments to better highlight the failure modes of a vertical plate anchor under a horizontal pull-out force (Dickin and Leung 1990).

Different methods, such as field and scaled models tests, numerical and analytical methods, have been proposed and practiced for analyzing and understanding the behavior of anchors. The large-scale field tests on foundations for transmission line towers and shafts

contributed the development of early empirical design methods (Giffels *et al.* 1960; Ireland 1963; Tucker 1987; Sutherland 1988). Scaled model tests have also been used to understand the failure modes of anchors in various anchor and soil conditions (Balla 1961; Vesic 1971; Ilamparuthi *et al.* 2002). Research on the vertical pullout of shallow anchor was initiated by Balla (1961). He obtained an equation for pullout resistance by solving Kotter's formula. Balla assumed the failure surface was a combination of a logarithmic spiral and a straight line.

Early theoretical researches on the behavior of anchors are mostly focused on the elastic response and the evaluation of the ultimate pull-out resistance (Fox, 1948; Douglas and Davis, 1964; Rowe and Booker, 1979). Many researchers have proposed different techniques based on either limit equilibrium concepts or the method of characteristics, frequently combined with empirical correlations, for determining the failure load of anchor plates (e.g. Balla, 1961; Meyerhof and Adams, 1968; Vesic, 1971; Ovesen and Stroman, 1972; Neely *et al.* 1973). All of these approaches involve some assumptions regarding either the shape of the failure surface or the influence of the soil above the anchor on the field of characteristics.

Meyerhof and Adams (1968) suggested a general solution of shallow and deep anchor by the theory of plasticity. Tagaya *et al.* (1988) indicated that there is good agreement between the theoretical and experimental values of the ultimate pull-out force of shallow anchors but for deep anchors the theoretical estimates are higher than the experimental values. Among various failure surfaces, there are mainly three distinctive failure modes proposed by various researchers, as shown in Fig. 1. The first failure surface is a frictional cylinder, as shown in Fig. 1a, which was first proposed by Majer (1955). The pullout capacity is equal to the weight of soil within the cylindrical failure surface directly above the anchor plus the frictional resistance along failure surface. Since the volume of the soil mobilized by an anchor is normally larger than the cylinder

above the anchor, the pullout capacity is most likely to be underestimated based on this failure surface. The second type of failure surface is a truncated cone, proposed firstly by Mors (1959), extending from the anchor with an apex angle of  $90^\circ + \varphi$ , where  $\varphi$  is the friction angle of the soil (see Fig.1b). The pullout capacity is calculated to be only the weight of the soil within the truncated cone. Mors' method is usually conservative for shallow anchors since it ignores the frictional force along the failure surface, but it overestimates the pullout capacity for deep anchor, where the failure surface normally does not extend to the ground surface and is smaller than the assumed truncated cone. The third type of failure surface is a circular surface extending from the edge of the anchor and intersecting the ground surface with an angle of approximately  $45^\circ - \varphi/2$ . This type of failure surface was proposed and used by Balla (1961) and also by Baker and Kondner (1966) in their calculations.

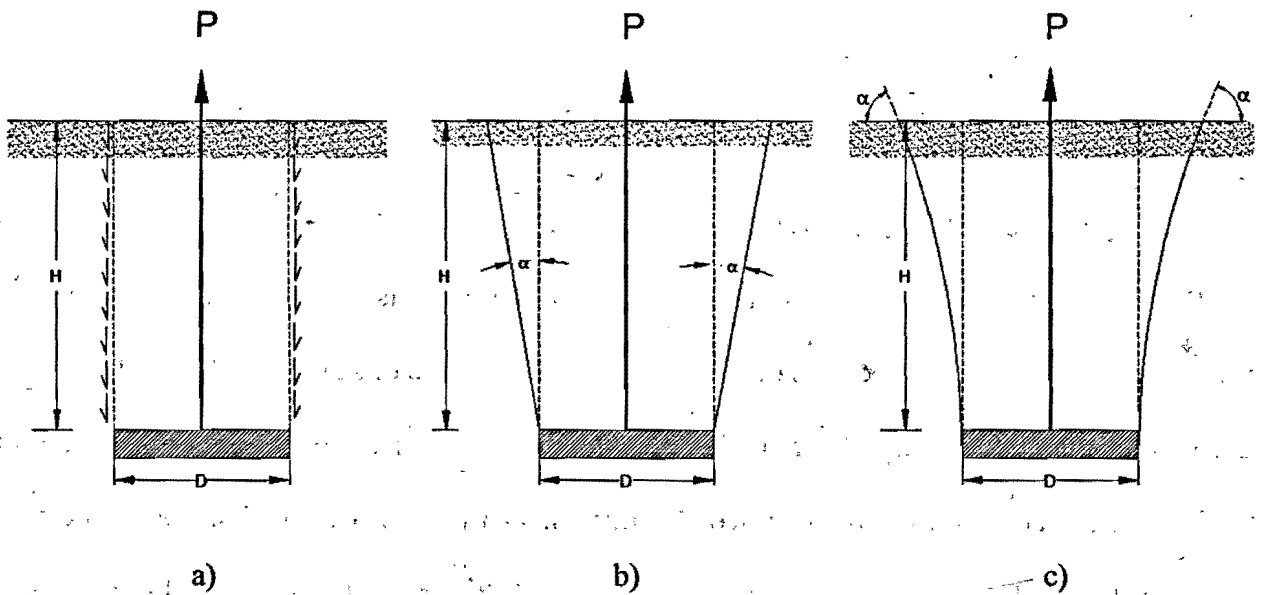


**Fig. 1** Three different failure modes in an earth anchor. (Liu *et al.* 2009)

Numerical methods including the finite element method (FEM) have also been used in studying anchors in both sand and clay. Rowe and Davis (1982) used finite element method to

simulate and analyze a strip anchor in sand, and found that the dilatancy could significantly influence the ultimate pullout resistance. Sakai and Tanaka performed FEM analysis of shear band development for a circular anchor in sand (Sakai and Tanaka 2007). They studied the behavior of anchor plates in sand using an elasto-plastic finite element analysis and compared the results with their experimental data. Most recent design methods are based on either assumed or experimental failure surfaces in small-scale model tests at unit gravity.

## 1.2 Applications

Anchoring has a broad range of application in the petroleum industry where many offshore structures are built for the purpose of oil/gas extraction. In some cases the offshore platforms operate in significant depths of water, as illustrated in Fig. 2. In deep waters, anchors are required to hold offshore platforms in position by transferring the uplift forces to the seabed. In shallow waters, anchorage is used to fix these types of structures in their place (fixed platforms) and effectively utilize them in operation.

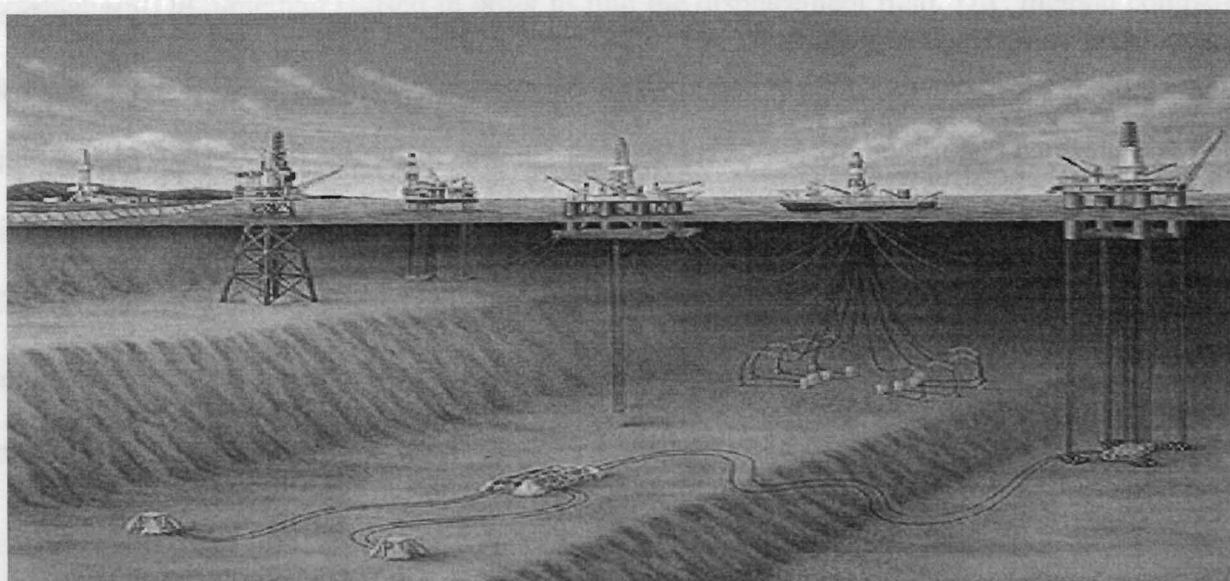


**Fig. 2-** Offshore structures and anchorage (U.S Mineral management services 2007)

Anchoring can also be used in combinations with other stabilization techniques. For example, as illustrated in Fig. 3, in tunnels or caverns a combination of shotcrete or fiber mesh and anchors could be an effective way to stabilize the soil (Anchor-Shotcrete Method).

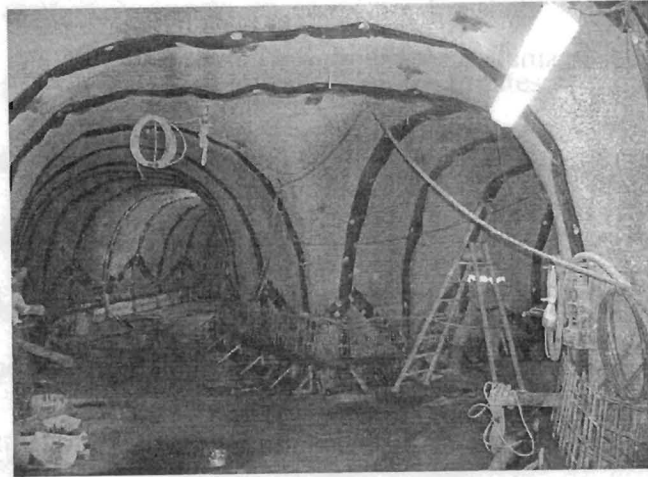


**Fig. 3-Anchoring of Caverns and Tunnels (Picture from bridgat Inc.)**

Plate capacities and anchor types (see Fig. 4) are generally selected based on the shape of the failure surface.

Anchoring allows relatively easy selection on the source of static analysis of the value, direction, and the load centre of the anchoring forces, with maximum effect and economy. Anchor plates are structural elements often used to hold up tensile forces performing on structures such as retaining walls or sheet piles.

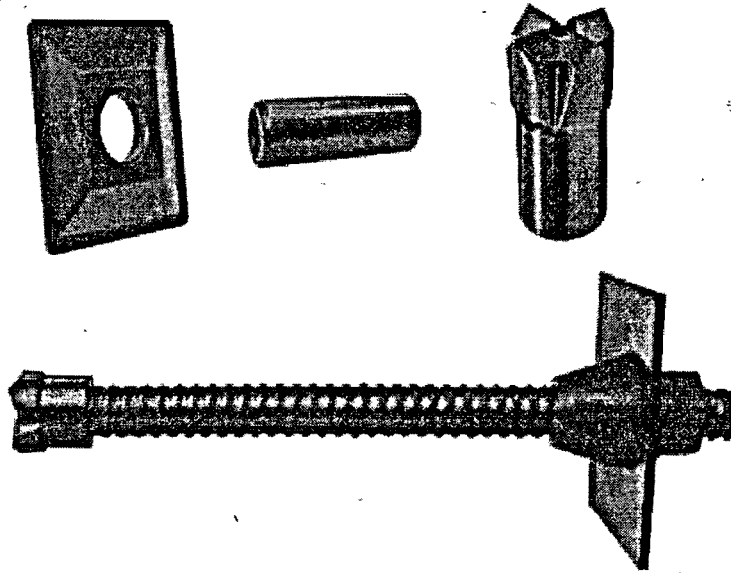


Fig. 4- Self drilling Anchorage (Picture from bridgat Inc)

### 1.3 Scope and Study Method

The focus in this study is on the behavior and failure modes of a deep anchor embedded in sand. A scaled model test has been developed for this purpose and the digital image correlation (DIC) method is used in order to find the displacement field. DIC method compares any two consecutive images to find the deformation field. In addition, schematic finite element analyses have been carried out to provide more insight into the failure mechanisms and their associated displacement fields. The report also includes a parametric study on the influential factors such as embedment depth of the anchor and density of the sand. The results in both dense and loose sand are compared with each other to better distinguish between the different failure modes.

## CHAPTER 2

### SOIL PROPERTY AND EXPERIMENT SETUP

#### 2.1 Experimental Set-up

As it was mentioned earlier, in this project a scaled anchor model test is used to investigate the mechanical behavior and failure modes of a deep anchor embedded in sand. The components of the scaled model developed in this research are as follows.

- 1- **Camera:** The camera is a Complementary Metal Oxide Semiconductor (CMOS) PL-B741E model, with a resolution of 1280 x 1024 pixels from PixeLink (3030 Conroy Road, Ottawa, ON, K1G 6C2, Canada). Transmission was provided via standard CAT6 consumption, with high-speed, superior anti-blooming, flexible cables. A Matlab program/code was developed to run and control the camera.
- 2- **Plexiglas Mould:** As illustrated in Fig. 5, to be able to monitor and photograph the displacement field around the anchor the model box is made of Plexiglas. The box is 500mm long, 300mm wide and 500mm deep.

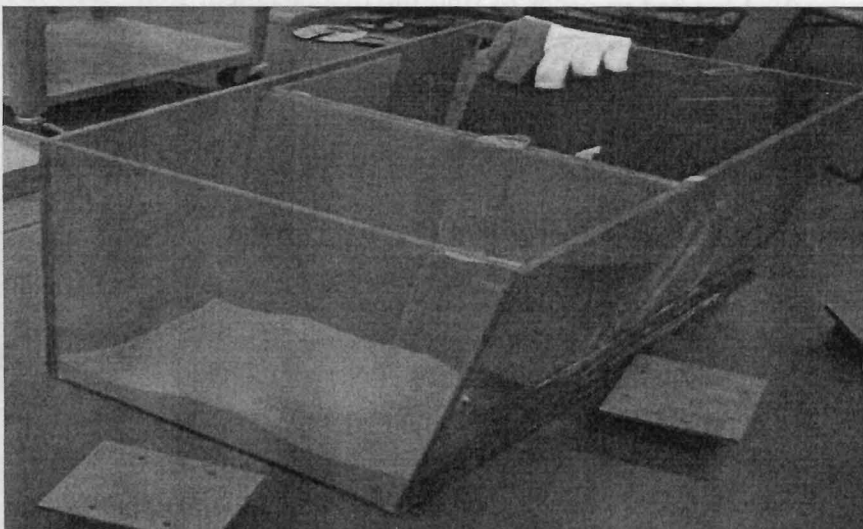


**Fig. 5-** Plexiglas mould with the dimensions of 500\*300\*500 mm

- 3- **Semicircular Anchor:** A semicircular anchor with a diameter of 50.8 mm and a thickness of 5 mm was used in this study.
- 4- **Threaded Steel Rod:** To uplift the anchor a 1000 mm long threaded steel rod with a diameter of 5 mm was used to connect the semicircular anchor at the bottom to the load cell at the top.
- 5- **Load cell:** In order to measure the uplift force, a load cell (see Fig. 6), with the loading capacity of 890N, was connected to a loading frame at one end and to the steel rod at the other end.



**Fig. 6-** Load cell was connected to a computer to register changes in force

- 6- **Linear Variable Differential Transformer (LVDT):** The LVDT used here had a linear stroke of  $\pm 25$  mm. The LVDT was installed on a plate connected to the loading frame to measure the displacement of the rod and consequently the uplift of the anchor. A typical LVDT, as shown in Fig. 7, is a variable-reluctance device, where a primary center coil establishes a magnetic flux that is coupled with a mobile armature to a symmetrically-wound secondary coil on either side of the primary. The strong relationship between core position and output voltage yields a sensor design that shows excellent resolution, limited more by the associated circuitry than the sensing method (Pierson-2001).

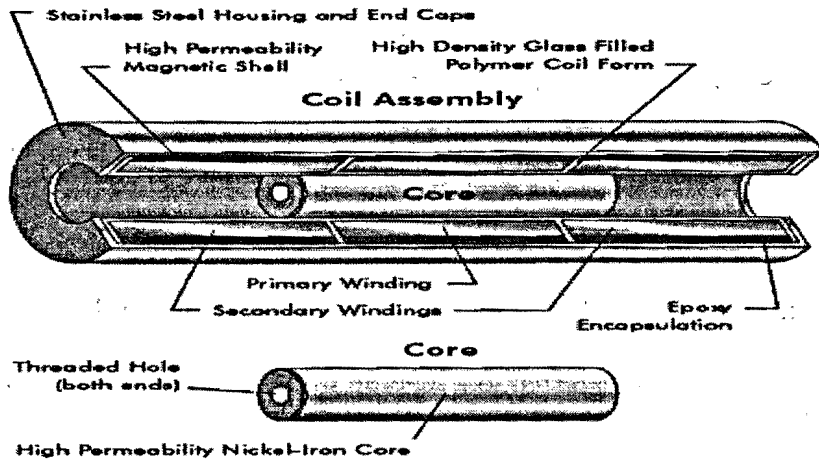


Fig. 7- Components of a typical LVDT

- 7- **DC Current Supplier:** The load cell and LVDT were supplied by a DC current. In order to get the correct data and result, proper voltage had to be applied to the load cell and LVDT.
- 8- **Loading Frame:** The loading mechanism, load cell and the LVDT was assembled on a loading frame as shown in Fig. 8. The uplifting load was applied to anchor by a screw mechanism. The anchor was lifted upward with a constant displacement rate of approximately 3 mm/min along a frictionless guide slot by manually rotating the handle. The guide slot was connected to the loading frame using four clamps, and the rod could move inside of the guide slot without any restraint. A view of the complete setup is presented in Fig. 9.

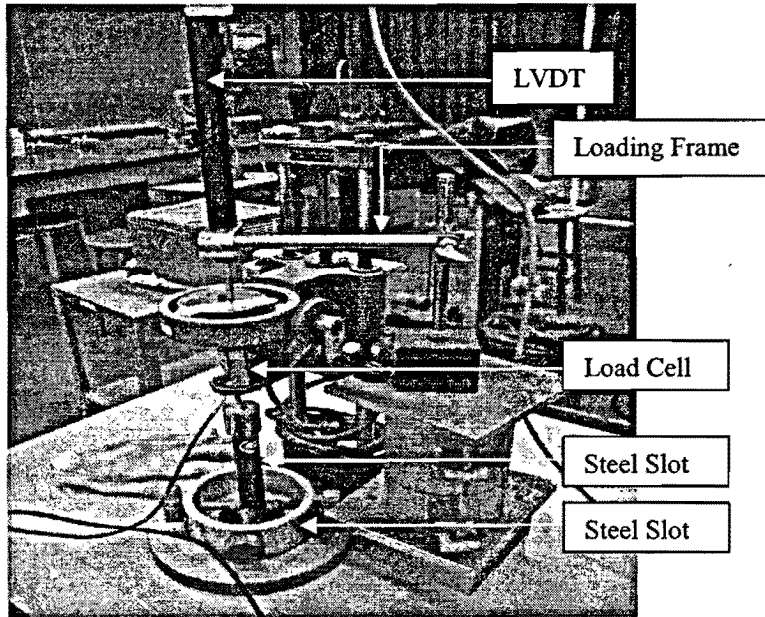


Fig. 8- Installation of LVDT and load cell to loading frame table

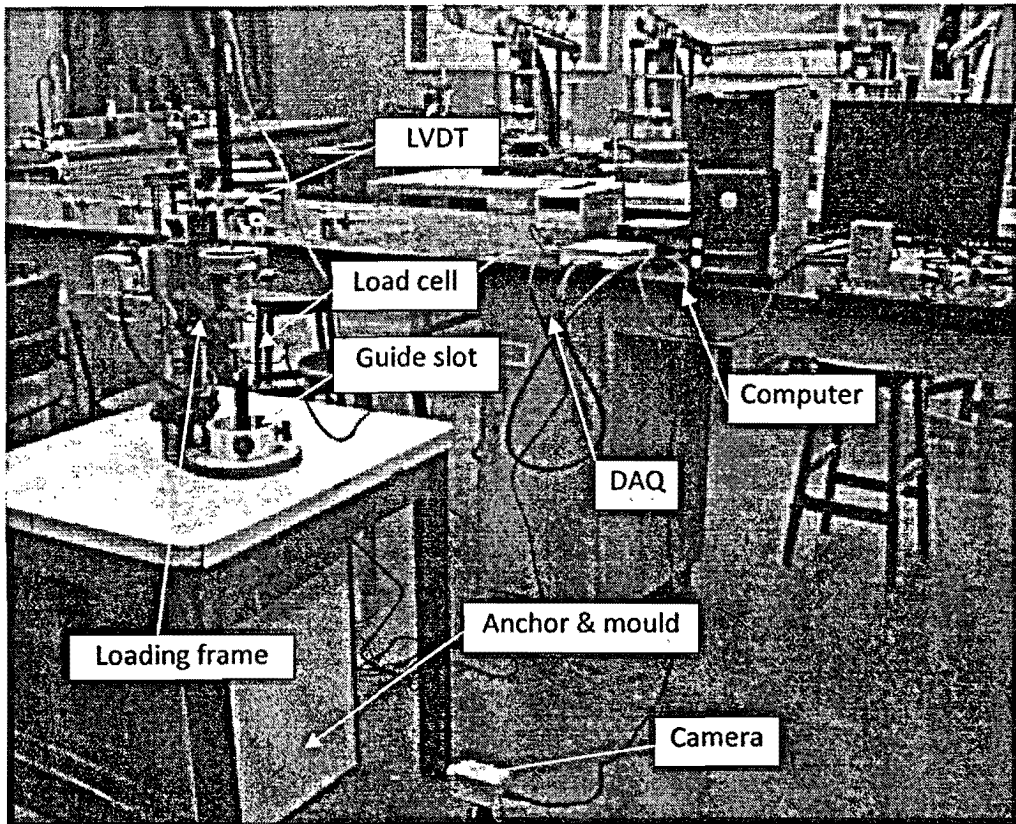


Fig. 9- Test set-up for anchor uplifting and image capturing

## 2.2 Soil Property

The material used in the model tests was uniformly graded fine sand that according to the United Soil Classification System is classified as SP. In order to investigate the effects of sand density the model test were prepared in both dense and mine loose conditions. From direct shear tests (ASTM D3080) performed in this study the angles of friction measured were  $30.0^\circ$  for fine loose (FL) and  $42.8^\circ$  for fine dense (FD) samples. The material properties of the sandy material at both loose and dense states are presented in Table 1. (Liu *et al.* 2009).

Table 1- Physical and Geotechnical properties of sand used in the tests

Soil parameters	Fine Sand	
	Loose (FL)	Dense (FD)
Uniformity coefficient, $C_u$	1.29	
Coefficient of curvature, $C_c$	0.98	
Effective grain size, $d_{10}$ (mm)	0.56	
Max dry unit weight, $\gamma_{dmax}$ (kN/m <sup>3</sup> )	16.5	
Min dry unit weight, $\gamma_{dmin}$ (kN/m <sup>3</sup> )	13.8	
Sample dry unit weight, $\gamma_d$ (kN/m <sup>3</sup> )	14.44-14.95	15.60-16.03
Relative density $D_R$ (%)	27-47	71-85
Peak angle of friction, $\phi$ (degrees)	30.0	42.8

## CHAPTER 3

### SCALED MODEL TEST PREPARATION

The steps of the model test preparation are as follows:

- 1- Cleaning the Plexiglas:** In order to take clear pictures, first the Plexiglas had to be cleaned properly.
- 2- Adjusting the rod on sand bed:** A 50mm deep sand bed was put in the mould. The semi-circular anchor was set on the sand bed and aligned vertically through the guide slot and horizontally against the front window of the Plexiglas mould. The centre line of the front sheet was marked to help positioning the semicircular anchor vertically. Adjusting the anchor near the center line of the mould increased the quality of the pictures (see Fig. 9).
- 3- Preparation of sand with the desired density:** For loose sand samples, the upper sand was prepared by the pulverization method to the desired height. For dense samples, the sand layers were compacted by tamping the sand layer by layer until the final height was reached. Based on the density measurements, as shown in Table1, the sample preparation method was fairly consistent in providing reproducible samples.
- 4- Connecting the rod to loading frame:** After filling the mold with sand the rod was connected to the loading frame for tests.

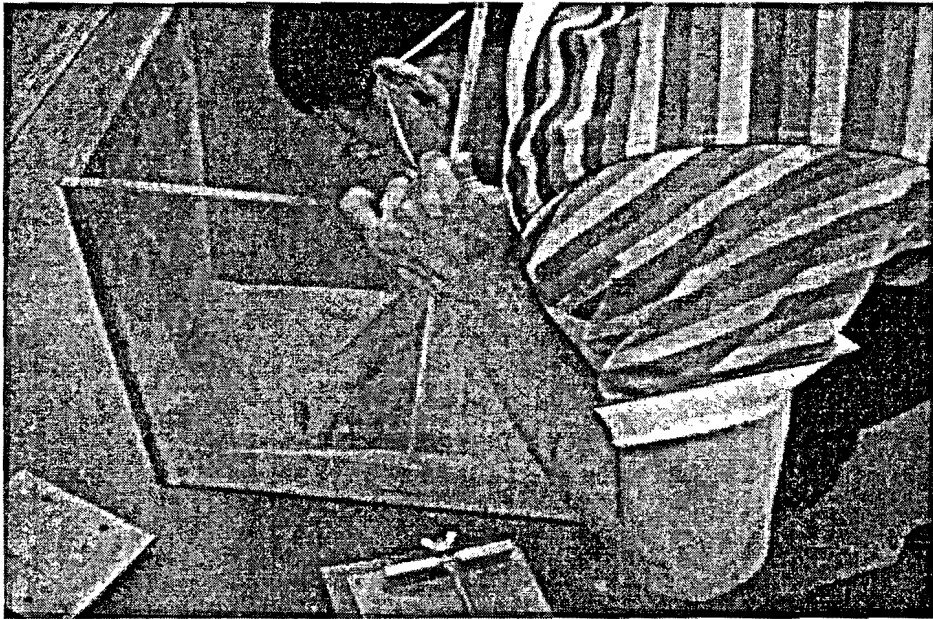


**Fig. 9-** Leveling the sand bed and positioning the rod at the centre of the Plexiglas sheet

**5- Adjusting the light:** Images were sensitive to changes in surrounding light therefore just one source of light was used to illuminate the surface of sand. All other lights in the laboratory were turned off during a test. The floor of laboratory in the vicinity of the model was covered with some clothes to eliminate the reflection of light from the floor.

**6- Setting up the camera:** The Camera was set up almost 400 mm away from the Plexiglas mould as shown in Fig. 10. The operation of the camera was controlled by a code written in Matlab programming language. The camera was set in Auto mode with the frame rate of one picture per second. Data acquisition was activated for recording the forces and displacements on the PC.

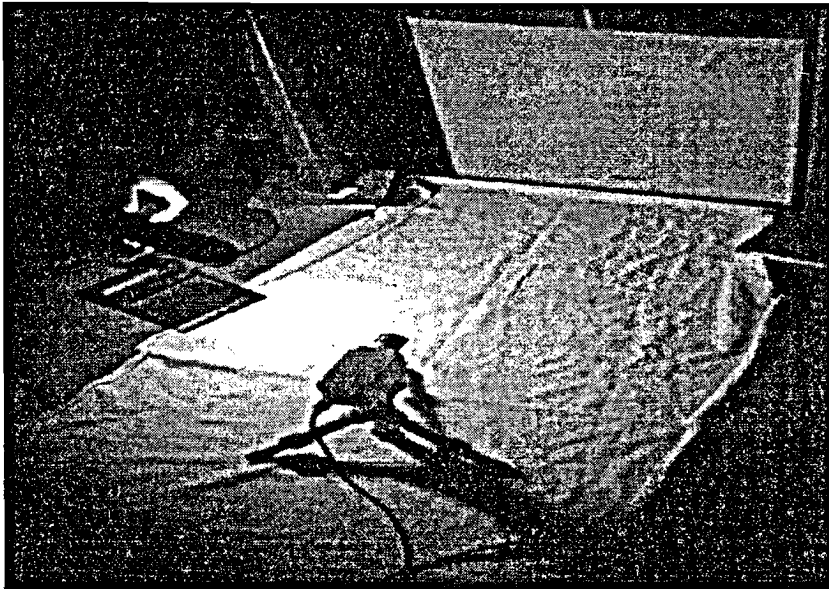


**Fig. 10-** Setting up camera and adjusting the light for test

**7- Uplifting the anchor:** Anchor was uplifted manually by rotating the handle of the screw mechanism while the images recorded by the camera and the load-displacement data collected by data acquisition system were stored in a computer. The rate of uplifting was maintained at approximately 3 mm/min while load-displacement data gathered through the load cell and the LVDT were saving automatically to the computer.

**8- Termination of the test:** The test was terminated when a visible failure surface was observed in the soil or when the accumulating vertical displacement would not result in any increase in the anchor pullout force.

## DIGITAL IMAGE CORRELATION PROCESSING TECHNIQUE

## 4.1 General Theory

Dislocation, displacement and strain measurements have been a challenge for engineers and designers for a long time. Digital image correlation techniques are getting more popular especially on micro and nano scales (Fig. 11). Simplicity in utilization and application is the major reason for the increasing popularity of this method. Developments in digital imaging have significantly improved the technology that supports the white-light method in the DIC approach.

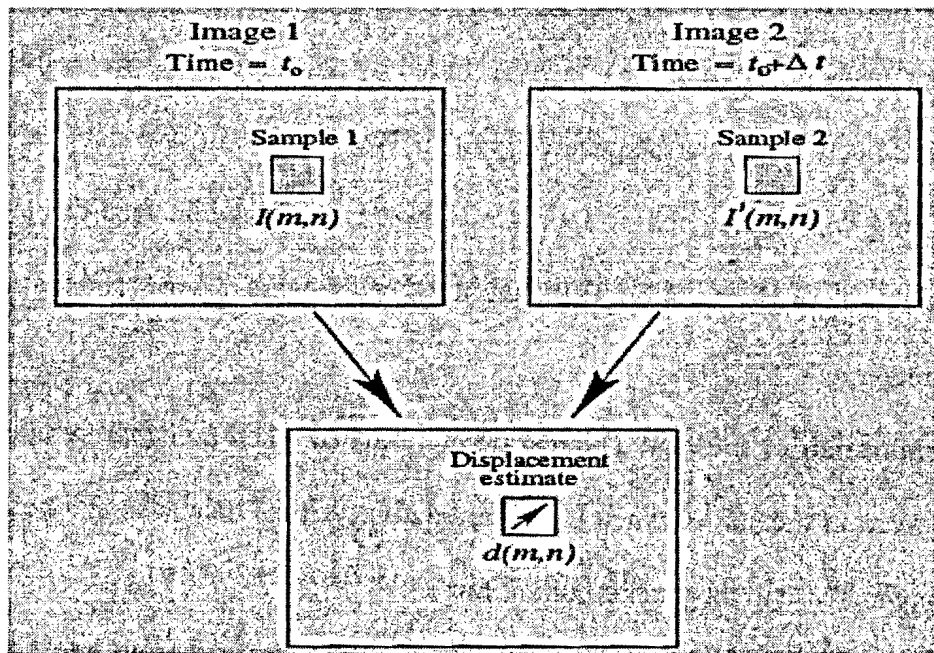


Fig. 11-Strain measuring or displacement estimate

This technique is applicable to many materials and model tests because it provides a wide range of markers and can be applied to measure a wide range of relative displacements. In this study a mathematical package (MATLAB) was used for the calculations involved in DIC.

## 4.2 Theory of DIC

In DIC, a set of adjacent points in the undeformed shape is assumed to remain adjacent after deformation. Fig. 12, illustrates schematically the deformation of an object. Quadrangle S dashed lines is a sub image in the reference or undeformed image, and quadrangle S1 solid lines is a sub image of the corresponding deformed image.

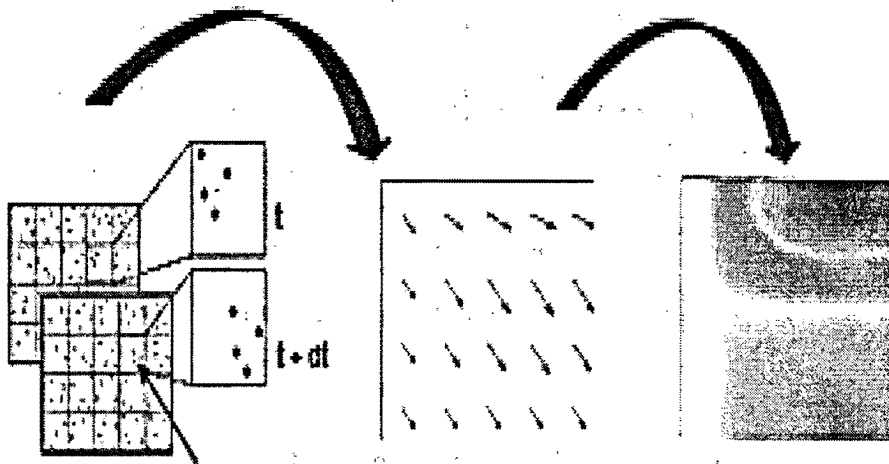


Fig. 12- Deformation vector field

In order to obtain the in-plane displacement  $u_m$  and  $v_m$  of point M, sub image S is matched with a corresponding sub image S1 using a correlation operation. If S is sufficiently small, the coordinates of points in S1 can be approximated by first-order Taylor expansion as follows:

$$x_{n1} = x_m + u_m + \left(1 + \frac{\partial u}{\partial x}\bigg|_M\right) \Delta x + \frac{\partial u}{\partial y}\bigg|_M \Delta y, \quad (1)$$

$$y_{n1} = y_m + v_m + \frac{\partial v}{\partial x}\bigg|_M \Delta x + \left(1 + \frac{\partial v}{\partial y}\bigg|_M\right) \Delta y, \quad (2)$$

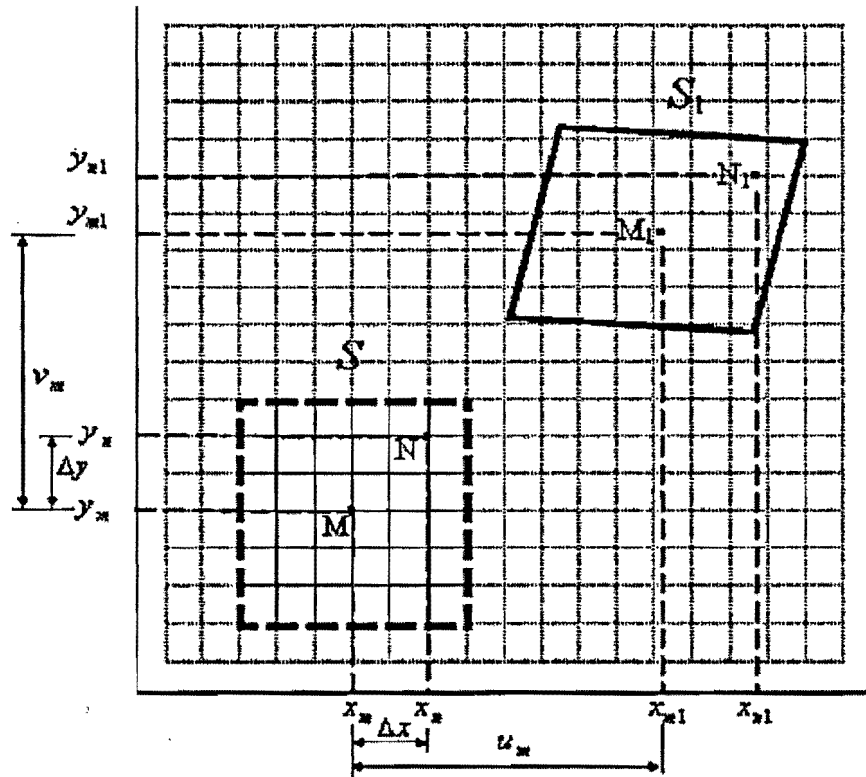


Fig. 13- Schematic deformation of an object

The distinct form of standard cross-correlation function is as follows:

$$C(\Delta x, \Delta y) = \frac{1}{MN} \sum_{m=0}^{M-1} \sum_{n=0}^{N-1} f(m, n) g(m + \Delta x, n + \Delta y) \quad (3)$$

Where  $f$  and  $g$  are the grayscale intensities of two images being interrogated,  $M$  and  $N$  are the dimensions of two interrogated images. If the cross-correlation has a peak value at a location of  $(x_p, y_p)$ , then the best match of  $f$  and  $g$  occurs when  $g$  is shifted such that its origin is located at  $(x_p, y_p)$ . (Liu *et al.* 2009)

Let  $f(x, y)$  and  $f_d(x, y)$  be the gray-value distributions of the undeformed and the deformed image, respectively. For subset  $S$ , auto-correlation coefficient  $C$  is defined as

$$C = \frac{\sum_{N \in S} [f(x_n, y_n) - f_d(x_{n1}, y_{n1})]^2}{\sum_{N \in S} f(x_n, y_n)^2} \quad (4)$$

Where  $(x_n, y_n)$  is a point in subset S in an undeformed image, and  $(x_{n1}, y_{n1})$  is a corresponding point defined by equations (1) and (2) in subset S1 in a deformed image. It is clear that if parameters  $u_m$  and  $v_m$  are the real displacements and  $\partial u/\partial x$ ,  $\partial v/\partial x$ ,  $\partial u/\partial y$ ,  $\partial v/\partial y$  are the displacement derivatives of point M, the correlation coefficient  $C$  will be zero. Hence minimization of the coefficient,  $C$ , would provide the best estimates of the parameters.

Minimization of the autocorrelation coefficient,  $C$ , is a nonlinear optimization process and Newton-Raphson or Levenburg-Marquardt iteration method are usually used in the implementation of the process (Y. H. Huang *et al.* 2005).

It has to be noted that the resolution of the camera plays an important role in the accuracy of assessment of the pictures.

### 4.3 Data Processing

Collected pictures were processed by PIVview software. This software was used with 'Quick-Look', particle image velocimetry (PIV) analysis, during and after PIV experiments. This program has interactive features for image examination as well.

Other features of the software are:

- Cross-correlation, autocorrelation and speckle-shift analysis modes
- Supports TIFF, BMP, JPEG, B16 (16bit PCO), PNG, PBM, and other image formats
- Image pre-processing
- Image batch processing
- Multiple pass, multiple grid algorithms
- Ensemble correlation
- High precision processing

- Batch and command-line processing
- Extensive outlier treatment
- Interactive calibration
- Stereo-PIV calibration and processing
- Data export in TecPlot, netCDF and ASC-II
- Plot export
- Post-Processing: filters, velocity, strain
- PDF/HTML-based documentation

## CHAPTER 5

### RESULT ANALYSIS

#### 5.1 Theoretical Solution to the Anchor Problem

The average applied pullout pressure  $q_u$  required to cause failure of an anchor plate in a cohesionless soil with the angle of friction  $\phi$ , may be expressed in the form of

$$q_u = \gamma h F'_\gamma \quad (5)$$

where  $\gamma$  is the unit weight of the soil,  $h$  is the depth to the bottom of the anchor and  $F'_\gamma$  is an anchor capacity factor which is a function of the orientation, the embedment ratio, the angle of friction, dilatancy of the soil, the initial stress state and the anchor roughness. The embedment ratio is defined as the ratio of the depth of burial over the diameter of the anchor.

$F'_\gamma$  could be expressed approximately in terms of a basic anchor capacity factor  $F_\gamma$  and a number of correction factors, i.e.

$$F'_\gamma = F_\gamma R_\psi R_R R_k \quad (6)$$

where  $F_\gamma$  is the anchor capacity factor for the basic case of a smooth anchor resting in a soil that deforms plastically with no volume change (dilatancy angle  $\psi = 0$ ) and with a coefficient of earth pressure at rest  $k_0 = 1$ .  $R_\psi$ ,  $R_R$  and  $R_k$  are correction factors for the effects of soil dilatancy, anchor roughness and initial stress state, respectively.

Sutherland (1965) found that the failure mode changes with changes in sand density and also stated that Balla's (1961) analytical method was only accurate for loose to medium-dense sands. Sutherland et al. (1982) suggested a theory for shallow and deep anchor conditions plane failure surface, where  $\theta$  was a function of relative density and  $\phi$ .

## 5.2 Model Test Results of an Anchor in Dense Sand

The results of model tests of an anchor embedded in dense sand, with different embedment ratios, are presented in this section.

### 5.2.1 Force vs. Displacement in Dense Sand

The data gathered from the load cell and LVDT were used to plot the load-displacement behavior. Fig. 14 presents the force-displacement characteristics for deep anchors, with the embedment ratios of 6, 7, 8 and 9, in dense sand.

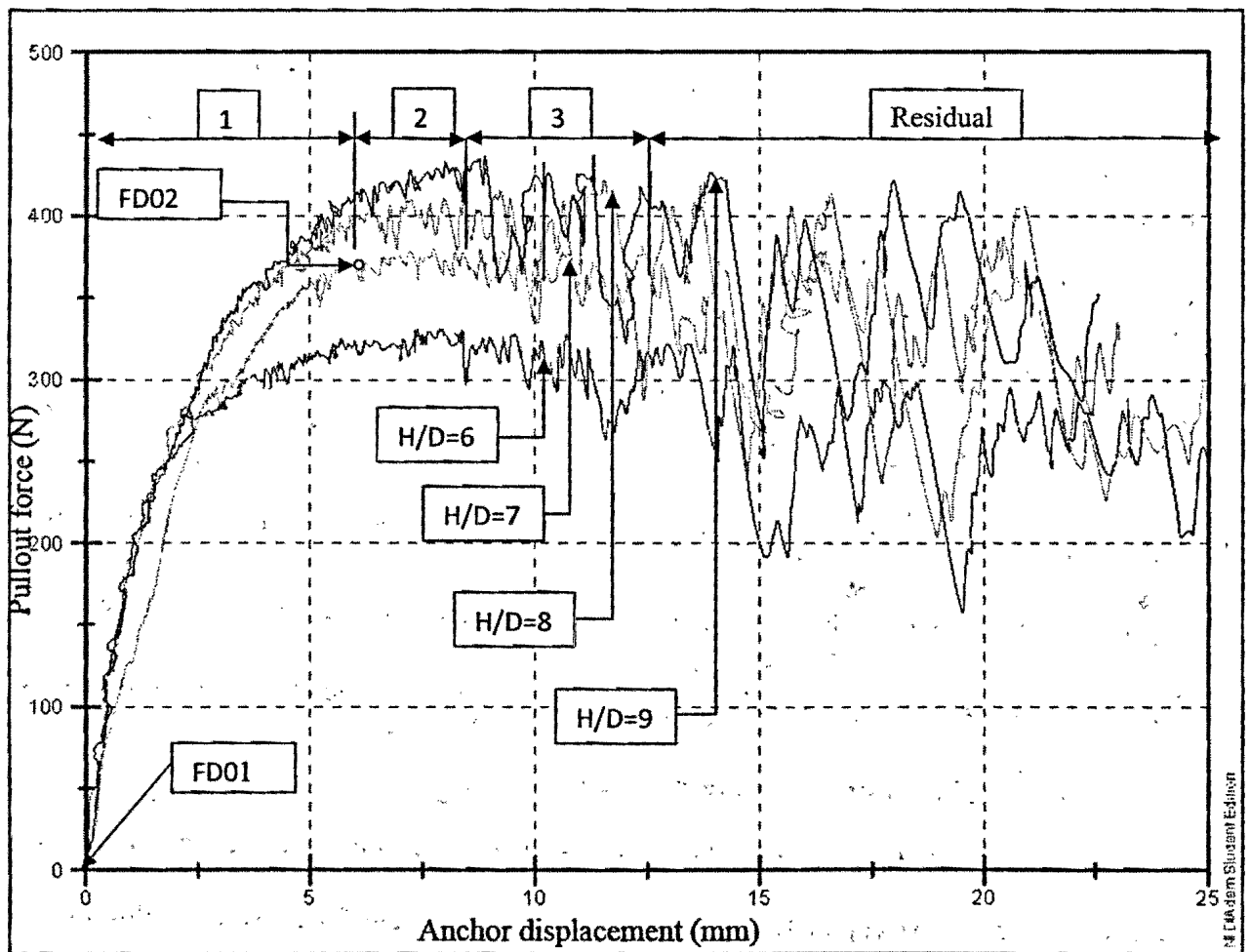


Fig. 14- Force-displacement characteristics for deep anchors in dense sand

Considering that the diameter of the anchor was 50mm, the tests were conducted with burial depth of 300mm, 350mm, 400mm and 450mm, corresponding to an embedment ratio from 6 to 9.

To study the observed behavior first consider the case of  $H/D=7$ . The first stage in the load-displacement curve, marked as [1] in Fig. 14, is the pre-peak phase where the pullout resistance increases quickly. The maximum uplift force in this case is 365N at a vertical displacement of 6.30mm. The second phase, marked as [2], is called the post-peak. In this stage the slope of the load-displacement curve rapidly approach to zero, i.e. horizontal line. This means, comparing to the first phase, by increasing the vertical displacement the anchor pullout force will remain constant, except for the minor oscillations that are inevitable in an experiment. During the post- peak stage the uplift resistance oscillated slightly until the vertical displacement reached to approximately 10mm. The last phase observed in Fig. 14, marked as [3], represents the residual state. At the residual phase, the recorded pullout resistance had considerable oscillations.

A similar pattern was observed for other values of the embedment ratios. For the anchor with  $H/D=9$  a maximum pullout force equal to 430N was obtained at a vertical displacement of 7mm. The second phase is constrained to a narrow range of displacements and in the last phase of the experiment, compared to the case of  $H/D=7$ , one can observe more pronounced oscillations in the uplifting resistance.

For the anchor with  $H/D=6$ , the maximum uplift force is 320N and it corresponds to vertical displacement of 7.5mm. The oscillations in the uplifting resistance were recorded when vertical displacement was about 12 mm.

In all the curves shown in Fig. 14, the oscillations in pullout resistance started at the end of the post peak stage. This event started at lower values of vertical displacement for higher values of embedment ratio.

The failure displacement is defined as the displacement at which the pullout resistance reaches its peak value. Since the material is cohesionless, the upward movement of the anchor creates an empty space right beneath the anchor plate. This empty space in turn is filled by the local collapse and movement of the sand in the vicinity of the anchor plate. This is the reason for the oscillation observed in the load-displacement curves.

### **5.2.2 Displacement Field in Dense Sand Using DIC Method**

The deformation field in one of the model tests is presented in Fig. 15. Clearly in dense sand the failure surface is a curved cone extended from the edges of the anchor to the soil surface, similar to what was schematically shown in Fig. 1b and Fig. 1c. The middle block, the area surrounded by two lines labeled BR and BL, was fully mobilized and bounded by two shearing zones on both sides.

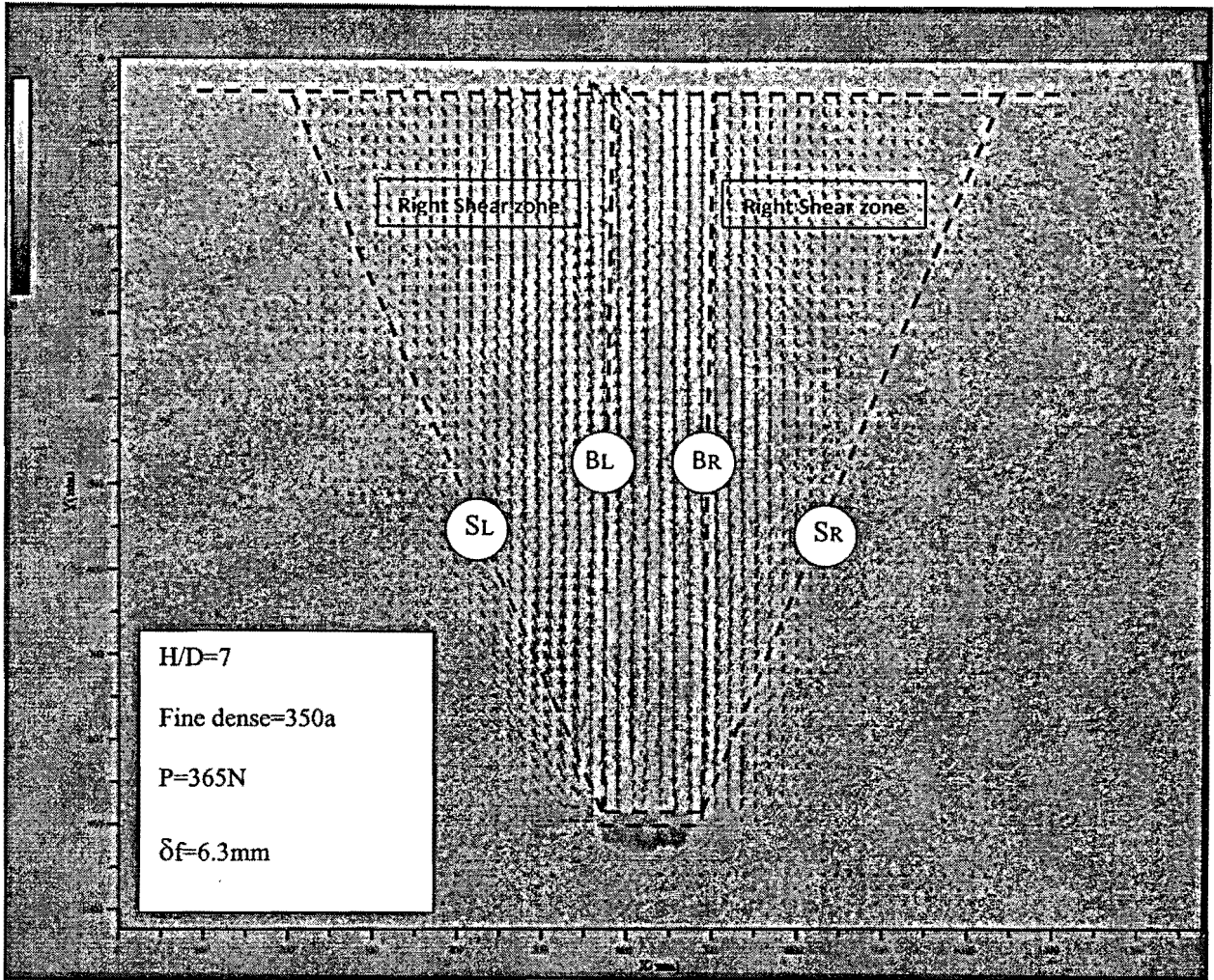


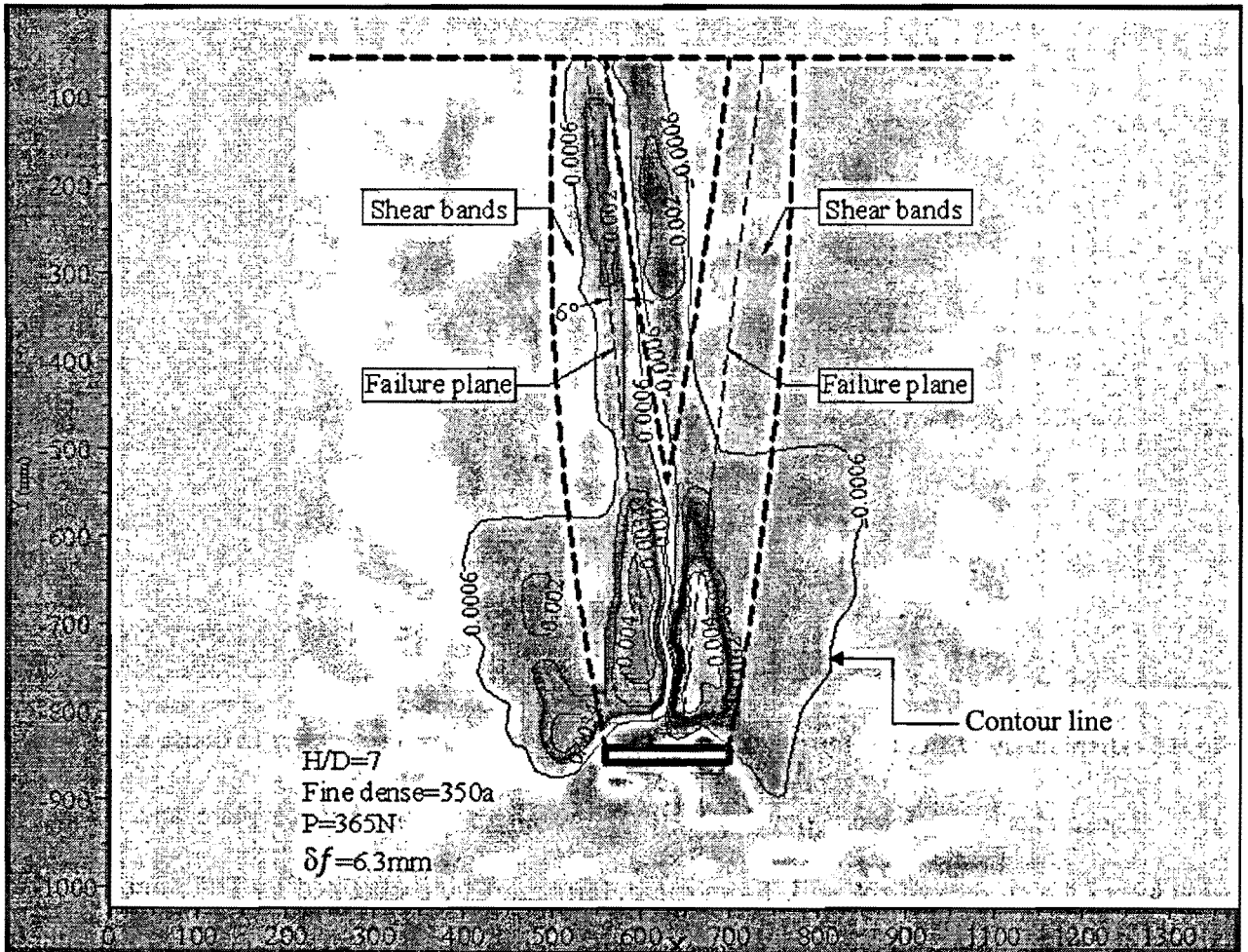
Fig. 15- Displacement field at the maximum pullout resistance of the anchor in dense sand

These shear zones were developed from the edges of the anchor plate and gradually extended to the surface of the soil. From the deformation field obtained by DIC, one can also calculate the variation of shear strain in the whole domain.

### 5.2.3 Shear Strain in Dense Sand

The results presented in Fig. 16 show the contours of shear strain around the same deep anchor in dense sand. Fig. 16 demonstrate that the magnitude of shear strain has a much higher value right above the anchor.

Shear strain is almost in the same range on two third of the length of the rod, which is marked by contours by the PIVview software. Clearly the shear zones are extended from the edges of the anchor to the surface of the soil.



### 5.3 Model Test Results of an Anchor in Loose Sand

The results of model tests of an anchor embedded in loose sand, with different embedment ratios, are presented in this section.

#### 5.3.1 Force vs. Displacement in Loose Sand

Data gathered from the load cell and LVDT was processed and the following curves were obtained from the model tests of an anchor embedded in loose sand. The force vs. displacement curves of an anchor in loose sand with different values of embedment ratios are presented in Fig. 17. Similar to the case of dense sand, the embedment ratios are 6 to 9. The same three phases that were observed in Fig. 14 for the case of dense sand can be identified in Fig. 17 for loose sand. The major difference is in the values of the uplift resistance.

For example considering the anchor with the embedment ratio of  $H/D=9$ , in dense sand the maximum pullout force was 430N obtained at 8mm vertical displacement, while in loose sand the maximum pullout force is 90N at 6mm of vertical displacement. This indicates that the anchor capacity is significantly affected by the density of the material.

The softening behavior in the post peak phase is more intense for the case of dense sand. In other words the pullout resistance maintained its peak value for a wider displacement range in loose sand. No appreciable softening happened in loose sand.

For both graphs in Figs. 14 and 17, the oscillations in the pullout force started when the vertical displacement was about 8mm.

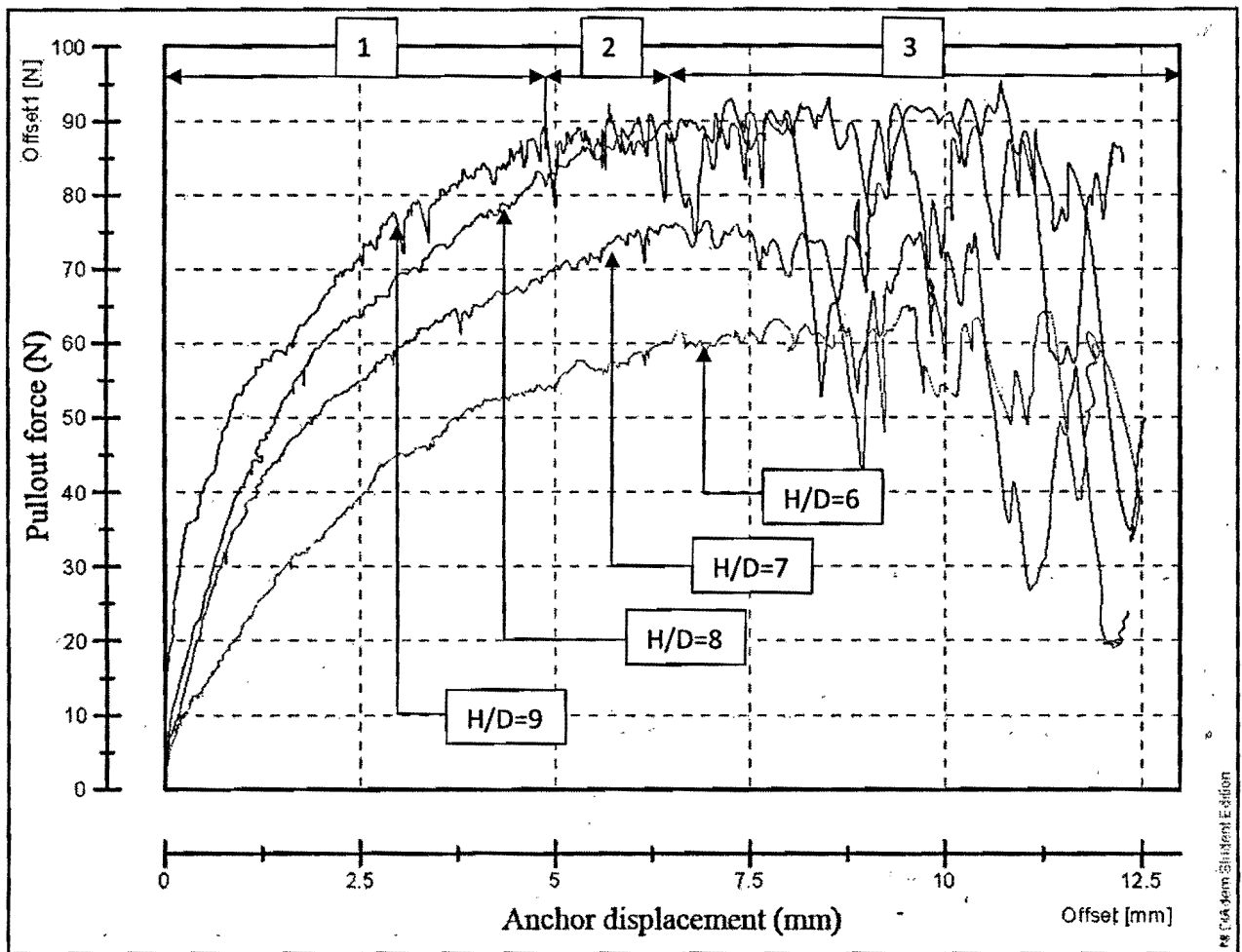


Fig. 17- Force vs displacement for deep anchors in loose sand

### 5.3.2 Displacement Field in Loose Sand Using DIC Method

The deformation field in one of the model tests on loose sand is presented in Fig. 18. Clearly in loose sand the soil displacement did not extend to the surface of the sand. A significant deformation occurred within a bell-shaped influence zone, which extended from the anchor plate to a distance about two times the anchor diameter above the anchor. Based on the gradient change in soil displacement, a significant compaction was noticed in this influence zone.

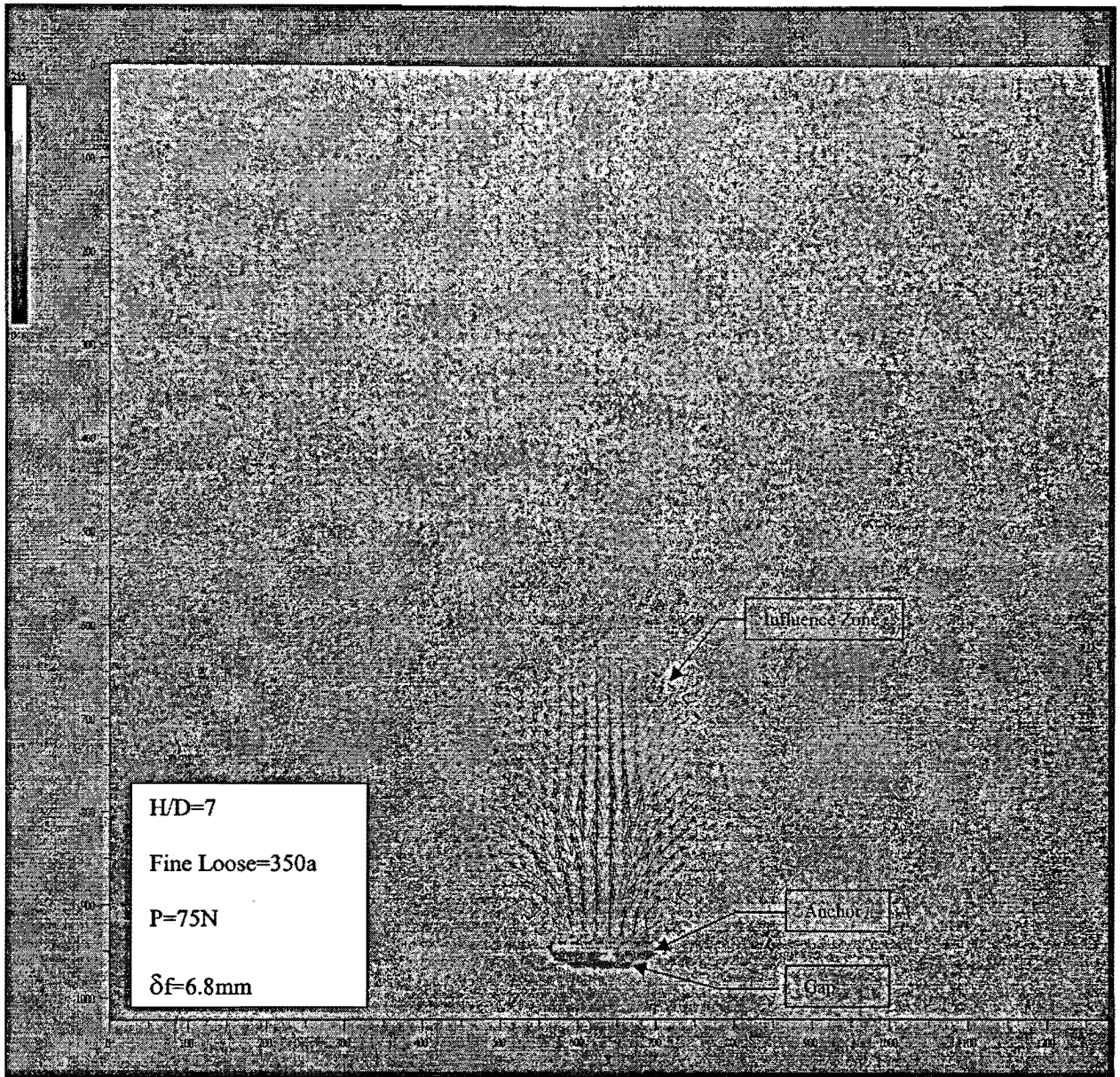


Fig. 18- Displacement field at the maximum pullout resistance of the anchor in loose sand

The failure modes and the influence zones observed in Figs. 15 and 18 can be explained by the volumetric behavior of dense and loose sand used in the tests. Loose sand has a tendency to be compacted under (shear) loads. That is the reason majority of the force in the experiments was mobilized just to relocate the sand particles and compact the sand in the vicinity of the anchor plate. Under dense condition, sand has a tendency to dilate, i.e. show increase in volume

under (shear) loads. Because of this in the tests on dense sand the area affected by anchor displacement covers a wider region of the model.

### 5.3.3 Shear Strain in Loose Sand

From the deformation field obtained by DIC one can calculate the variation of shear strain in the whole domain. The results presented in Fig. 19 show the contours of shear strain around the deep anchor in loose sand.

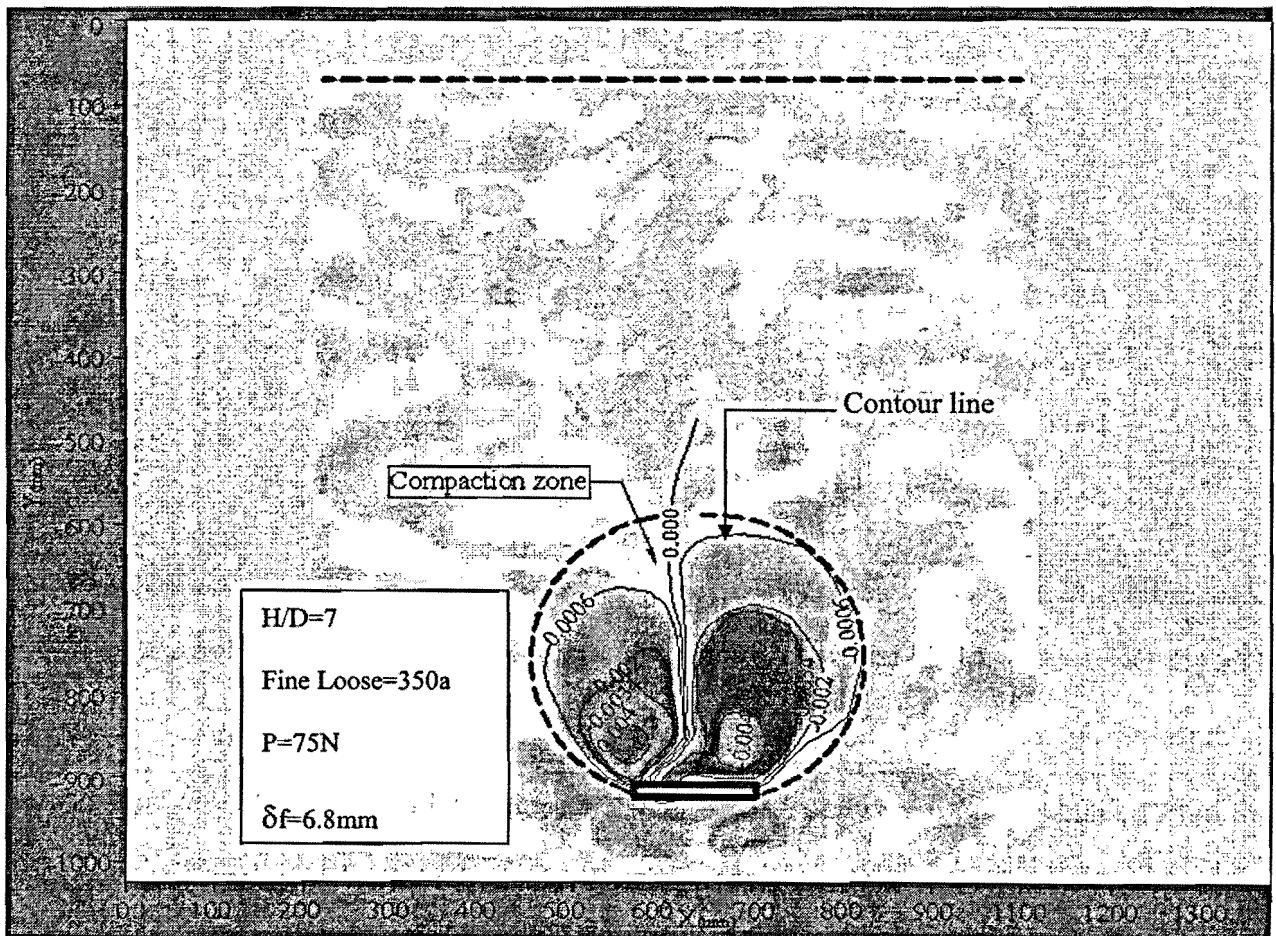


Fig. 19- Shear strain in loose sand

Similar to the case of dense sand, the maximum shear strain occurred right around the anchor. As it can be seen in Fig. 16 for dense sample, shear strain around the rod existed all

along its length. It started from around the anchor and it is finished at the surface of the soil. In contrast, from Fig. 19 it is observed that there is an inconsistency in shear strain distribution around the anchor in loose sand.

#### 5.4 A comparison between pullout resistance in this research study and the work of others

An extensive review on the anchor resistance obtained from field and model tests by many researchers is presented in an article by Ilamparuthi et al. (2002). In order to compare the results obtained from various studies, the pullout resistances in various tests under different conditions are normalized to a dimensionless breakout factor, i.e.

$$N_{qf} = \frac{Q_f}{\gamma'AH} \quad (6)$$

where  $N_{qf}$  is the dimensionless breakout factor,  $Q_f$  is the pullout resistance,  $\gamma'$  is the effective unit weight of sand,  $A$  is the area of the anchor plate and  $H$  is the depth of burial. Based on the collected experimental results they have also proposed some empirical equations for estimating the breakout factor from the geometry of the anchor, the depth of burial, the void ratio, and the friction angle of the sand.

Fig. 20 presents the variation of breakout factor with the embedment ratio of anchors in loose sand. The results presented in this graph includes the data obtained by Kwasniewski *et al.* (1975) on loose sand with  $\varphi = 28^\circ - 32^\circ$ , Sutherland *et al.* (1982) on a medium dense sand with  $\varphi = 36.5^\circ$ , the predictions using the empirical relations proposed by Ilamparuthi et al. (2002) and

the experimental results obtained in this study on loose sand with  $\phi = 30^\circ$ . Clearly the experimental results obtained in this study are in the same range as reported by others.

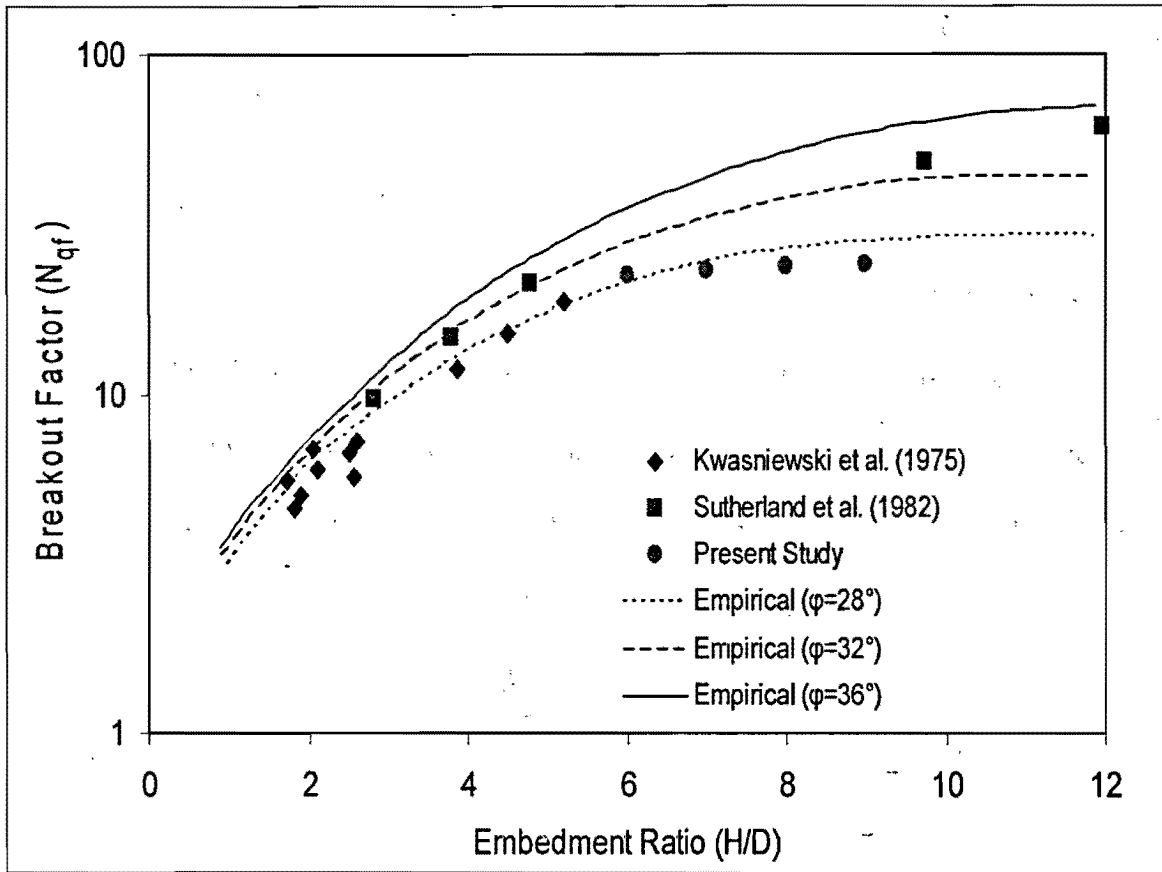
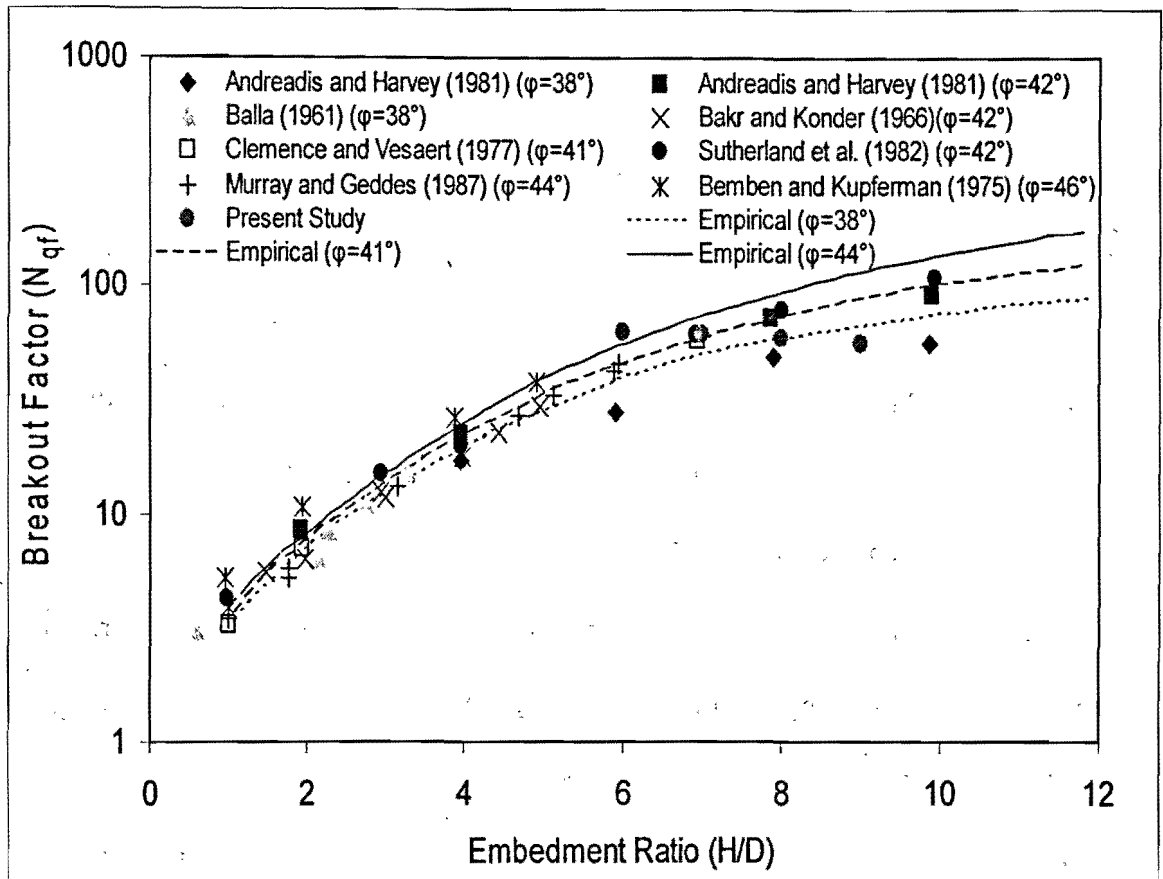


Fig. 20- Comparison of breakout factors of anchors in loose sand from previous experimental researchs, empirical relations and experimental results of the present study

For dense sand, where the friction angle is higher, a comparison between the experimental results from previous model studies (Andreadis and Harvey 1981; Balla 1961; Baker and Kondner 1966; Clemence and Veesaert 1977; Murray and Geddes 1987; Bembem and Kupferman 1975), the empirical relations (Ilamparuthi et al. 2002), and the results obtained in this study is presented in Fig. 21. In this graph the friction angle of dense sands is in the range of  $\phi = 38^\circ - 46^\circ$ . The dense sand used in this study has a friction angle of  $\phi = 42^\circ$ , within the study

range. Once again the experimental results obtained in this study are fairly close to the data obtained by other researchers.



**Fig. 21-** Comparison of breakout factors of anchors in dense sand from previous experimental researchs, empirical relations and experimntal results of the present study

## CHAPTER 6

### CONCLUSION

This report presents an experimental research on the failure modes of a deep anchor in loose and dense sand. The digital image correlation (DIC) technique was used in this investigation. The progress of sand movement during anchor lifting was photographed using a CMOS camera and later the images were analyzed by the DIC method. Through different scaled model tests performed in this study, the influence of soil density and the embedment depth on the failure modes of a deep anchor were studied.

Soil density had a significant influence on the failure mode of the anchor. Compared to clear failure planes extending from the anchor edges to soil surface in dense sand, a particularly different triangular wedge was developed in loose sand.

The pullout capacity was also greatly affected by sand density. The anchor experienced a much larger displacement through a significant compaction process before reaching the peak pullout resistance in loose sand compared to that of dense sand.

Both in loose and dense sands, the maximum shear strain were observed right around the anchor. There was inconsistency in shear strain around the anchor in loose sand. On the other hand, shear strain was consistent around the anchor in dense sand.

## REFERENCES

- Andreadis, A., and Harvey, R.C. (1981). A design procedure for embedded anchors. *Applied Ocean Research*, 3(4): 171-182.
- Baker, W.H., and Kondner, R.L. (1966). Pullout load capacity of circular earth anchor buried in sand. National Academy of Sciences, *Highway Research Board*, Report 108: 1-10.
- Balla, A. (1961). The resistance to breaking out of mushroom foundations for pylons. *Proc. of the 5th Int. Conf. on Soil Mechanics and Foundation Eng.*, Paris, France, 569-576.
- Bemben, S.M., and Kupferman, M. (1975). The vertical holding capacity of marine anchor flukes subjected to static and cyclic loading. *In Proceedings of the 7th Offshore Technology Conference*, Houston, Tex., OTC2185, 363-374.
- Clemence, S.P., and Veesaert, C.J. (1977). Dynamic pullout resistance of anchors in sand. *In Proceedings of the International Conference on Soil-Structure Interaction*, Roorkee, India, 389-397.
- Das B.M. (2002), *Principles of Geotechnical Engineering*, 5th Edition, Brooks/Cole.
- Dickin EA, Leung CF. (1983). Centrifugal model tests on vertical anchorplates. *J Geotech Eng Div*, 109: 1503-25
- Ghaly A, Hanna A. (1994). Ultimate pullout resistance of single vertical anchors. *Can Geotech J*, 31(5): 661-72.
- Giffels, W. C., Graham, R. E., and Mook, J. F. (1960). Concrete cylinder anchors. *Electrical World*, 154: 46-49.

- Ilamparuthi, K., Dickin, E. A., and Muthukrisnaiah, K. (2002). Experimental investigation of the uplift behaviour of circular plate anchors embedded in sand. *Canadian Geotechnical J.*, 39(3): 648-664.
- Ireland, H. O. (1963). Discussion on uplift resistance of transmission tower footings by E.A. Turner. *J. of the Power Division, ASCE*, 89(1): 115-118.
- Kwasniewski, J., Sulikowska, I., and Walter, A. (1975). Anchors with vertical tie rods. In *Proceedings of the 1st Baltic Conference, Soil Mechanics and Foundation Engineering*, Gdansk, Poland, 122-133.
- Leos Hobst and Josef Zajic. (1977). Anchoring in Rock. Research Institute of civil engineer, Brno, 20-31.
- Macdonald, H.F., (1963). Uplift resistance of caisson piles in sand. M.Sc. thesis, Nova Scotia Technical College.
- Murray, E.J., and Geddes, J.D. (1987). Uplift behaviour of plates in sand. *Journal of Geotechnical Engineering, ASCE*, 113(3): 202-215.
- Sakai, T., and Tanaka, T. (2007). Experimental and numerical study of uplift behavior of shallow circular anchor in two-layered sand. *J. of Geotechnical and Geoenvironmental Engineering*, 133(4): 469-477.
- Sutherland, H.B. (1965). Model studies for shaft raising through cohesionless soils. In *Proceedings of the 6th International Conference on SM and FE*, Montreal, Canada, vol. 2: 410-413.
- Sutherland, H. B. (1988). Uplift resistance of soils. *Geotechnique*, 38(4): 493-516.

- Sutherland, H.B., Finlay, T.W., and Fadl, M.O. (1982). Uplift capacity of embedded anchors in sand. In *Proceedings of the 3rd International Conference on the Behaviour of Offshore Structures*, Cambridge, Mass., 2: 451–463.
- Tagaya, K., Scott, R. F. and Aboshi, H. (1988). Pullout Resistance of Buried Anchor in Sand, *Soils and Foundations*, 28(3): 114-130.
- Telford, T., (1997). Anchorages and anchored structures. *Institution of Civil Engineers*. 39(3): 23-48.
- Tucker, K. D. (1987). Uplift capacity of drilled shafts and driven piles in granular soils. Foundations for transmission line towers. *ASCE GSP No.8*, New York.
- Vesic, A. S. (1971). Breakout resistance of objects embedded in ocean bottom. *ASCE Proc., J. of the Soil Mechanics and Foundations Division*, 97(9): 1183-1203.